

Catalysis of Elemental Sulfur Nanoparticles on Chromium(VI) Reduction by Sulfide under Anaerobic Conditions

YE QING LAN,^{*,†} BAOLIN DENG,^{*,‡}
CHULSUNG KIM,[§]
EDWARD C. THORNTON,^{||} AND
HUIFANG XU[⊥]

College of Sciences, Nanjing Agricultural University, Nanjing 210095, China, Department of Civil and Environmental Engineering, University of Missouri–Columbia, Columbia, Missouri 65211, Department of Environmental Science, University of Dubuque, Dubuque, Iowa 52001, Field Hydrology and Chemistry Group, Pacific Northwest National Laboratory (PNNL), Richland, Washington 99352, and Department of Geology and Geophysics, University of Wisconsin, Madison, Wisconsin 53706

Chromate (Cr^{VI}) reduction by sulfide was conducted in anaerobic batch experimental systems. The molar ratio of the reduced Cr^{VI} to the oxidized S^{-II} was 1:1.5 during the reaction, suggesting that the product of sulfide oxidation was elemental sulfur. Under the anaerobic condition, the reaction was pseudo first order initially with respect to Cr^{VI}, but the rate was dramatically accelerated at the later stage of the reaction. The rate acceleration was due to catalysis by elemental sulfur nanoparticles; dissolved species such as monomeric elemental sulfur and polysulfides appeared to be ineffective catalysts. Elemental sulfur nanoparticles were capable of adsorbing sulfide and such adsorbed sulfide exhibited much higher reactivity toward Cr^{VI} reduction than the aqueous-phase sulfide, resulting in the observed rate acceleration. Kinetic data under various reactant concentrations can be represented by the following empirical kinetic equation: $-d[\text{Cr}^{\text{VI}}]/dt = k_1 [\text{Cr}^{\text{VI}}][\text{H}_2\text{S}]^{0.63} + k_3 [\text{Cr}^{\text{VI}}][\equiv\text{S}-\text{SH}]^{0.57}$. The first term on the right-hand side corresponds to the noncatalytic pathway, with $k_1 = 1.0 \times 10^{-3} (\mu\text{M})^{-0.63} \text{ min}^{-1}$ at pH 7.60 and $8.2 \times 10^{-5} (\mu\text{M})^{-0.63} \text{ min}^{-1}$ at pH 8.10. The second term, $k_3 [\text{Cr}^{\text{VI}}][\equiv\text{S}-\text{SH}]^b$, is the catalytic term with $[\equiv\text{S}-\text{SH}]$ representing the adsorbed concentration of sulfide on the elemental sulfur nanoparticles (μM). The catalytic term is more important at the later stage of the reaction, as indicated by the observed kinetics and the enhancement of the reaction rate by externally added elemental sulfur nanoparticles. At pH 8.10, $k_3 = 0.0057 (\mu\text{M})^{-0.57} \text{ min}^{-1}$.

Introduction

Chromium is one of the most frequently detected soil and groundwater contaminants (1, 2). In aquatic environments,

chromium occurs mainly as species in the oxidation states of Cr^{VI} and Cr^{III}. Since Cr^{III} species are normally less mobile, the reduction of Cr^{VI} to Cr^{III} decreases chromium mobility and bioavailability. As a result, Cr^{VI} reduction has been used as an effective approach for chromium-contaminated site remediation.

Many chemicals are capable of reducing Cr^{VI} in the ambient aquatic environment by directly providing electrons, including zerovalent iron (3), divalent iron (4–6), hydrogen sulfide (7–9), and organic compounds (10–13). Rates of Cr^{VI} reduction depend on the types of reductants and solution pH. For example, Cr^{VI} reduction by Fe^{II} takes place rapidly, with the reaction rate decreasing from pH 1.5 to 4.5 and increasing from pH 5.5 to 8.7 (4, 14). The reduction by many organic compounds is slow near neutral pH, but the rate normally increases as pH is decreased (15). Once reduced, Cr^{III} species are quite stable. The only compounds known to oxidize Cr^{III} to Cr^{VI} in the subsurface environment are manganese oxides (16–19).

There are many other chemical constituents that may not directly reduce Cr^{VI} but can alter the rate of Cr^{VI} reduction. Deng and Stone (12, 13) investigated surface-catalyzed Cr^{VI} reduction on goethite ($\alpha\text{-FeOOH}$), aluminum oxide ($\alpha\text{-Al}_2\text{O}_3$), and titanium dioxide by various organic reductants, including α -hydroxyl carboxylic acids and their esters, α -carbonyl carboxylic acids, and substituted phenols. Their research revealed that the rate of Cr^{VI} reduction could be increased by several orders of magnitude in the presence of some metal (hydr)oxides. In another study, Buerge and Hug (20) found that Cr^{VI} reduction by Fe^{II} was strongly enhanced by iron minerals, including goethite and lepidocrocite. Dissolved metals such as Mn^{II}/Mn^{III}, Fe^{II}/Fe^{III}, and Cu^{II}/Cu^I were also able to catalyze Cr^{VI} reduction (21, 22).

Cr^{VI} reduction by hydrogen sulfide takes place rapidly in a wide range of pH, with the reaction being explored as a remediation approach for chromium immobilization in the subsurface (8). The reaction with sulfide may also contribute to Cr^{VI} reduction in natural water and sediments (7). Under anaerobic conditions, elemental sulfur is the main product of sulfide oxidation by chromate (9), manganese oxide (23), and ferric iron (24). In aerobic systems, elemental sulfur is an important intermediate of sulfide oxidation by oxygen (25, 26). It is well-established that elemental sulfur reacts with hydrogen sulfide to form polysulfides, primarily tetrasulfide (S₄²⁻) and pentasulfide (S₅²⁻), under ambient temperature (25, 27–29). Elemental sulfur is considered to be insoluble in water, with the solubility of $\alpha\text{-S}_8$ being only 5 $\mu\text{g/L}$ at 20 °C (30), so the elemental sulfur product may precipitate when the solubility product is exceeded. The formation of elemental sulfur sols, or nanoparticles, is controlled by the nucleation and sulfur diffusion for the particle growth (31, 32).

This study aimed to evaluate the catalytic effects of elemental sulfur nanoparticles on Cr^{VI} reduction, similar to other mineral surfaces. The reaction kinetics and mechanism were investigated through batch experiments conducted under strictly controlled anaerobic conditions.

Materials and Methods

Chemicals. Solutions were prepared by deionized Milli-Q water (Q-H₂O, with 18.2 M Ω ·cm resistivity, Millipore Corp.) after purging with high-purity nitrogen gas for at least 20 min. Glassware was cleaned by soaking in 1 M HCl for at least 3 h and then thoroughly rinsing with Q-H₂O. Potassium dichromate, elemental sulfur (S₈), diphenyl carbazide, acetone, and *N,N*-dimethyl-1,4-phenylenediamine oxalate were

* Corresponding authors phone: (573) 882-0075; fax: (573) 882-4784; e-mail: dengb@missouri.edu or lanyq102@yahoo.com.cn.

[†] Nanjing Agricultural University.

[‡] University of Missouri–Columbia.

[§] University of Dubuque.

^{||} PNNL.

[⊥] University of Wisconsin.

purchased from Aldrich Chemical Co., and boric acid, sodium phosphate, sodium hydroxide, sodium sulfide ($\text{Na}_2\text{S}\cdot 9\text{H}_2\text{O}$), sulfuric acid, ferric chloride, and diammonium hydrogen phosphate were from Fisher Scientific. The chemicals were at least ACS reagent grade and mostly used without further purification, but sodium sulfide crystals were rinsed with degassed $\text{Q-H}_2\text{O}$ to remove the oxidized surface layer. Stock solutions of chromate and sulfide were stored in amber bottles placed in an anaerobic chamber (Models 855-AC, PLAS-LABS, Inc.) prior to use. Elemental sulfur stock suspension was prepared using crystalline elemental sulfur (S_8) powder dispersed in acetone.

Experimental Systems. Experiments reported in this study were mostly performed in the anaerobic chamber (N_2 , balanced by 10% H_2), including experimental setup, sample collection, and chemical analyses. Solution pH was controlled by 0.10 M phosphate buffer (pH 7.60) or 0.10 M borate buffer (pH 8.10). No strong electrolytes were applied to control ionic strength in this study, since the literature (7, 33) and our preliminary experiments all indicated that the reaction was independent of ionic strength when it was between 0.0 and 1.0 M. The actual ionic strength in the experimental systems was mainly controlled by the buffer solutions, which was less than 0.10 M.

To ensure no sulfide loss due to evaporation, adsorption, and oxygenation, we tested the stability of sulfide at pH = 7.60 and 25 °C. First, approximately 40 mL of 0.10 M phosphate buffer was added into a 41 mL amber bottle and degassed with high-purity N_2 for 20 min; then the bottle was placed into the anaerobic chamber. After sulfide stock solution was pipetted into the buffer solution, the bottle was tightly closed by a screw cap with a Teflon liner and mixed by hand. Samples (0.50 mL) were taken at 30 min intervals with a 0.5 mL glass syringe for sulfide analysis. Sulfide was found to be stable for at least 180 min at 200 μM concentration level and at least 120 min at 800 μM concentration level. Kinetic experiments in this study followed a similar procedure with a sulfide concentration ranging from 200 to 800 μM and an experimental time period within 200 min.

Reaction stoichiometry between Cr^{VI} and $\text{S}^{-\text{II}}$ was determined by monitoring the consumption of both reactants with different initial concentration ratios. The temperature was maintained at 15 ± 0.5 or 25 ± 0.5 °C using a water bath.

Kinetic experiments were conducted by monitoring the change of Cr^{VI} concentration as a function of time in excess sulfide over Cr^{VI} . At pH 7.60, tests were performed with initial Cr^{VI} concentrations ranging from 10 to 60 μM and initial sulfide concentrations from 300 to 800 μM . The temperature varied in the range of 5–35 °C. For experiments at pH 8.10, $[\text{Cr}^{\text{VI}}]_0$ and $[\text{S}^{-\text{II}}]_0$ were maintained at 40 and 800 μM , respectively.

As detailed in Results, the rate of Cr^{VI} reduction by H_2S was accelerated at a later stage of the reaction. Our hypothesis was that some reaction intermediates/products might have catalyzed the reaction. Three types of experiments were performed to diagnose whether elemental sulfur produced during Cr^{VI} reduction by $\text{S}^{-\text{II}}$ could be the catalyst: (1) After 40 μM Cr^{VI} was completely reduced in a system with 800 μM total sulfide, another 40 μM Cr^{VI} was re-spiked into the system. The rationale was that if elemental sulfur was involved in the Cr^{VI} reduction, the reduction rate of the re-spiked Cr^{VI} should be enhanced by the elemental sulfur produced from the previous batch of reaction. (2) After 40 μM Cr^{VI} was completely reduced in a system with 800 μM total sulfide, the supernatant solution was collected by centrifugation at 6000 rpm (IEC Clinical Centrifuge, International Equipment Co.), followed by filtration through 0.40 μm Millipore membrane filters. The supernatant was degassed with N_2 again and in the anaerobic chamber, re-spiked with predetermined amounts of Cr^{VI} and S^{II} . The purpose was to see whether the removal

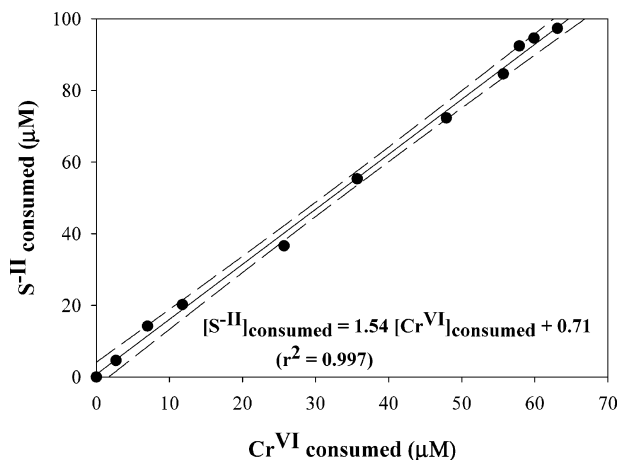


FIGURE 1. The consumption of $\text{S}^{-\text{II}}$ versus Cr^{VI} during the reaction under the anaerobic system ($[\text{S}^{-\text{II}}]_0 = 100 \mu\text{M}$; $[\text{Cr}^{\text{VI}}]_0 = 200 \mu\text{M}$; pH = 7.60; 25 °C).

of solid products could have any effects on the subsequent Cr^{VI} reduction. (3) Elemental sulfur was added into the buffer solution prior to the additions of Cr^{VI} and $\text{S}^{-\text{II}}$. The hypothesis was that if it was the elemental sulfur product that catalyzed further Cr^{VI} reduction, the externally added S^0 should similarly demonstrate such catalysis. Elemental sulfur was prepared in acetone to allow proper dispersion and formation of elemental sulfur nanoparticles, similar to the procedure of preparing hydrophobic sulfur sols (31, 32). In the reaction systems, the acetone concentration was always less than 2%. Control experiments showed that, at this concentration level, acetone did not alter the reaction rate between Cr^{VI} and $\text{S}^{-\text{II}}$.

Analytical Methods. Cr^{VI} concentration was determined by the diphenylcarbazide colorimetric method, using phosphoric acid buffer to control pH for the color development (13, 34). The absorbance was measured in a 1 cm cell at 540 nm on a spectrophotometer (Spectronic 20 Genesys, Spectronic Instruments). The method detection limit was 0.05 μM . Sulfide concentration in the stock solution was measured with the standard iodometric titration method (34). Sulfide concentration during the reaction was monitored by the methylene blue colorimetric method with the absorbance measured at 664 nm (34, 35). Calibration curves for the methylene blue method were linear in sulfide concentration from 0 to 15 μM and from 15 to 40 μM , with $R^2 > 0.998$ for both concentration ranges.

Solution pH was measured before the initiation and after the completion of reaction by an Orion 420A pH meter after two-point calibration. The pH of the buffered solution remained constant during the reaction. Dissolved oxygen in the N_2 -purged water was analyzed in selected experiments using the HACH dissolved oxygen test kit (HACH Co., Loveland, CO) to check completeness of oxygen removal by N_2 purging.

Transmission electron microscopy (TEM) was used for the imaging of elemental sulfur particles. A drop of solution containing the S particles was placed on a holey carbon coated Cu grid. The Cu grid was placed on TEM specimen holder after the Cu grid dried. All TEM observations were carried out with a JEOL 2010 high-resolution transmission electron microscope (HRTEM) with an Oxford Instruments LINK EDS system (36).

Results

Stoichiometry. Reaction stoichiometry was determined by plotting the amount of $\text{S}^{-\text{II}}$ oxidized versus the amount of Cr^{VI} reduced during the reaction. Cr^{VI} reduced was linearly related to the amount of $\text{S}^{-\text{II}}$ oxidized for the system initially containing 100 μM $\text{S}^{-\text{II}}$ and 200 μM Cr^{VI} (Figure 1). Such linear

TABLE 1. Regression Lines for S^{-II} Oxidized (Y) vs the Cr^{VI} Reduced (X) during the Reaction at Various Initial Reactant Concentrations (pH 7.60) and Temperatures, with the Slope Representing the Molar Ratio of [S^{-II}]_{ox}/[Cr^{VI}]_{red}, with Uncertainties Indicated at the 95% Confidence Level

temp (°C)	[S ^{-II}] ₀ (μM)	[Cr ^{VI}] ₀ (μM)	regression lines	R ²
15	100	40	Y = (1.49 ± 0.26)X - 0.28	0.9625
15	100	200	Y = (1.60 ± 0.08)X - 0.38	0.9968
25	100	200	Y = (1.54 ± 0.06)X - 0.72	0.9972
25	100	40	Y = (1.53 ± 0.13)X - 2.74	0.9894
25	100	40	Y = (1.44 ± 0.22)X - 0.42	0.9769

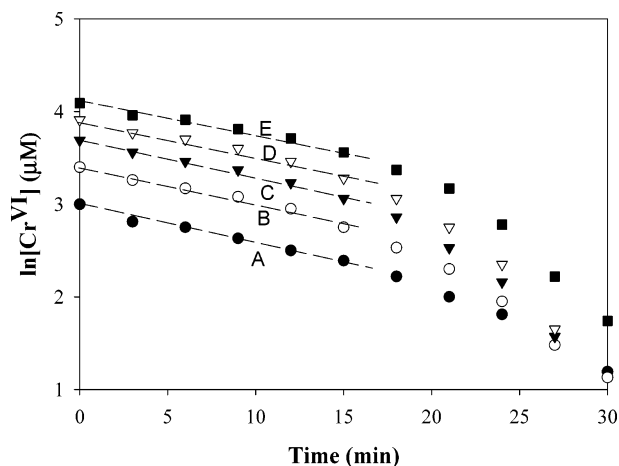
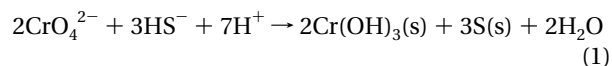


FIGURE 2. $\ln [Cr^{VI}]$ as a function of time in the systems with excess sulfide (800 μM) at pH = 7.60 and 25 °C. ([Cr^{VI}]₀: (A) 20, (B) 30, (C) 40, (D) 50, and (E) 60 μM.)

plots were obtained under other concentration and temperature conditions as summarized in Table 1, with R² all greater than 0.96. The slopes of these linear lines represented the molar ratios of S^{-II} and Cr^{VI} consumed during the reaction, which ranged from 1.44 to 1.60 with an average of 1.52. Based on a Student *t*-test, the measured molar ratio was statistically the same as 1.50. Since three electrons were involved for the reduction of Cr^{VI} to Cr^{III}, the molar ratio of 1.5 obtained here indicated that each sulfide provided two electrons on average; so S⁰ was likely the reaction product of S^{-II} oxidation, in agreement with an earlier report where elemental sulfur was directly identified by TEM with associated energy dispersive spectroscopy (9). Effort was made to detect sulfate using the BaSO₄ turbidity method (34), but the sulfate concentration was all below the detection limit (ca. 10 μM). These results thus indicated that the reaction took place according to the following reaction stoichiometry:



Kinetics. Typical kinetics behavior for Cr^{VI} reduction was illustrated by plotting the logarithm of [Cr^{VI}] versus time under various initial Cr^{VI} concentrations (Figure 2). All systems had a [S^{-II}]₀ at least 13 times higher than [Cr^{VI}]₀. The plots were all linear at the initial stage of the reaction, characteristic of a pseudo-first-order dependence on Cr^{VI}. Such linear $\ln [Cr^{VI}]$ vs *t* plots have been reported in the literature (7, 9, 33). To our surprise, the lines in our systems were significantly curved downward at the later stage of the reaction; i.e., the Cr^{VI} reduction was greatly accelerated compared to the first-order kinetics. It also appeared that the higher initial Cr^{VI} concentration resulted in a larger acceleration.

To understand the reaction kinetics without the interference of reaction intermediates and products present at a

TABLE 2. Initial Rates of Cr^{VI} Reduction by Sulfide at Different Initial Reactant Concentrations

[S ^{-II}] ₀ = 800 μM		[Cr ^{VI}] ₀ = 20 μM	
[Cr ^{VI}] ₀ (μM)	initial rate (μM min ⁻¹)	[S ^{-II}] ₀ (μM)	initial rate (μM min ⁻¹)
10.0	0.87	300.0	0.67
20.0	1.71	400.0	0.76
30.0	2.17	500.0	0.91
40.0	2.18	600.0	1.09
50.0	3.47	800.0	1.24
60.0	4.02		

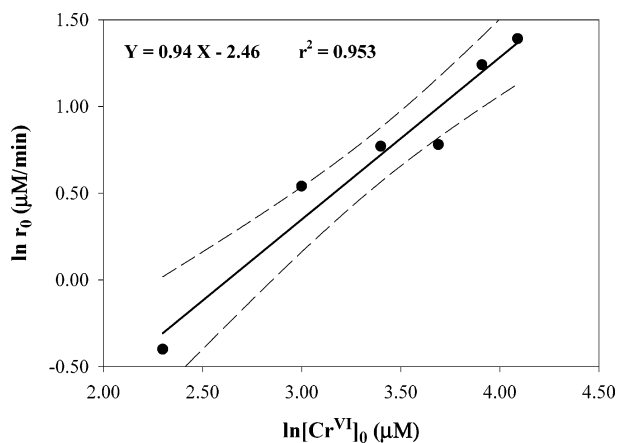


FIGURE 3. Initial rates at various initial Cr^{VI} concentrations in the excess of sulfide (800 μM) at pH = 7.60 and 25 °C. Dashed lines represent the 95% confidence level.

later stage of the reaction, initial rate methods were selected to calculate the reaction order (37), based on the data collected at an excess of [S^{-II}]₀ (800 μM) over [Cr^{VI}]₀ (10–60 μM). First, the data of Cr^{VI} concentration as a function of time was fitted by a polynomial equation; its first derivative was then evaluated at time zero to obtain the initial rates (*r*₀) (38) (see the results in Table 2). A linear $\ln(r_0)$ versus $\ln [Cr^{VI}]_0$ plot was obtained with a slope of 0.94 ± 0.29 (95% confidence level; Figure 3). The slope was very close to 1.00, indicating the reaction followed a pseudo-first-order kinetics with respect to Cr^{VI} at the initial stage of the reaction.

The initial rate method was similarly applied to calculate the reaction order with respect to S^{-II} based on the experiments performed at 20.0 μM [Cr^{VI}]₀ and various [S^{-II}]₀ (300–800 μM). The $\ln(r_0)$ versus $\ln [S^{-II}]_0$ plot (Figure 4) was linear with a slope of 0.67 ± 0.16 (95% confidence level). This fractional reaction order with respect to S^{-II} was slightly lower than the first-order kinetics reported in the literature (7, 9).

Effect of Elemental Sulfur. To our knowledge, rate acceleration for Cr^{VI} reduction by sulfide at a later stage of the reaction in reference to the first-order kinetics was not reported. Such acceleration was likely due to some types of intermediates and/or products formed during the reaction. Since elemental sulfur and chromium hydroxide were known to form in the experimental system, our working hypothesis was that the acceleration was due to these products. We examined Cr^{VI} reduction in the presence of 40 μM of Cr^{III} at pH 8.10. Equilibrium speciation calculation with the computer program MINEQL+ (39) indicated that the main Cr^{III} species was Cr(OH)_{3(s)} under the experimental condition. The test did not demonstrate any discernible effect of Cr^{III} on the reaction kinetics. Thus, the elemental sulfur produced during the reaction was proposed to be the main compound causing the accelerated Cr^{VI} reduction.

To confirm whether the elemental sulfur was indeed responsible for the catalysis, we first allowed 40 μM Cr^{VI} to

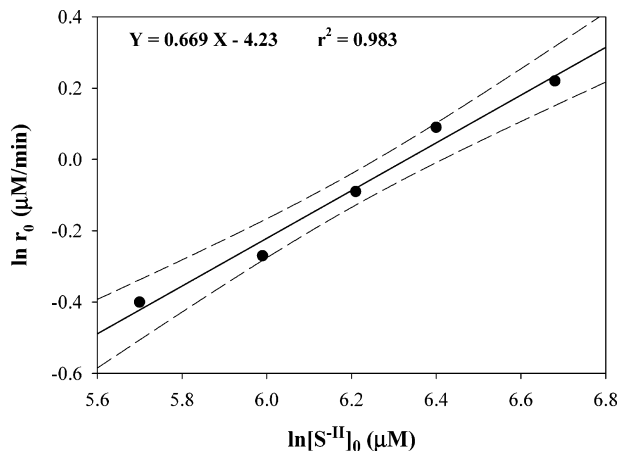


FIGURE 4. Initial rates at various initial S^{II} concentrations with constant $[Cr^{VI}]_0$ ($20.0 \mu M$; pH 7.60; $25^\circ C$). Dashed lines represent the 95% confidence level.

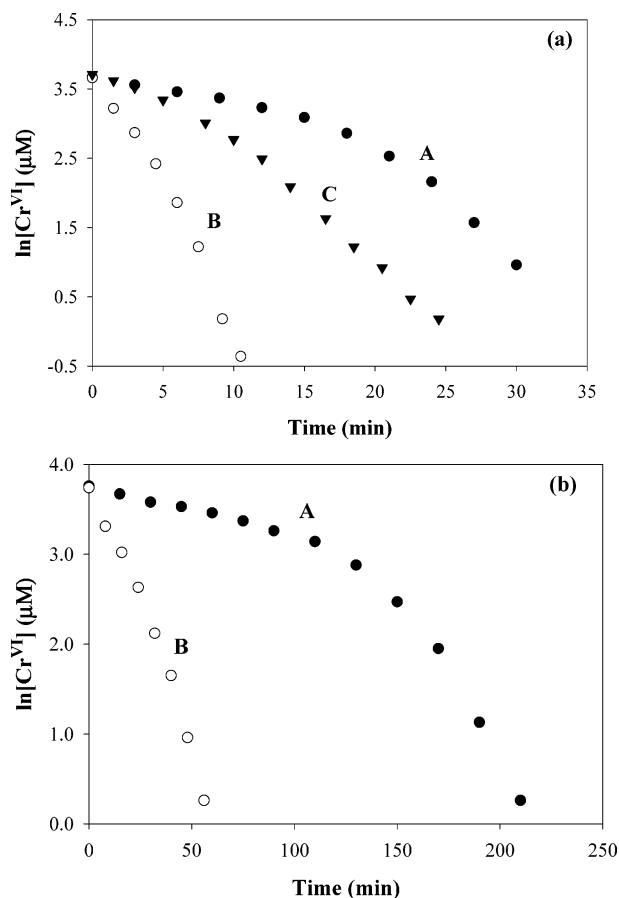


FIGURE 5. Time course plots for Cr^{VI} reduction at pH 7.60 (a) and pH 8.10 (b). Curve A: Reduction of first batch Cr^{VI} ($40 \mu M$) by S^{II} ($800 \mu M$). Curve B: Reduction of re-spiked Cr^{VI} after the reduction of the first addition is completed. Curve C: Reduction of re-spiked Cr^{VI} after the reduction of the first addition is completed and solid product is separated by centrifugation and filtration.

be completely reduced by $800 \mu M S^{II}$, and then additional Cr^{VI} was re-spiked directly. The results at both pH 7.60 (buffered by phosphate) and pH 8.10 (buffered by borate) were shown in Figure 5a,b, respectively. At pH 7.60 (Figure 5a), it took 21 min for a 69% Cr^{VI} reduction (from 40 to $12.6 \mu M$; curve A). During this process, it is expected that $41 \mu M$ of sulfide would be oxidized to elemental sulfur on the basis of the established reaction stoichiometry. When $40 \mu M Cr^{VI}$

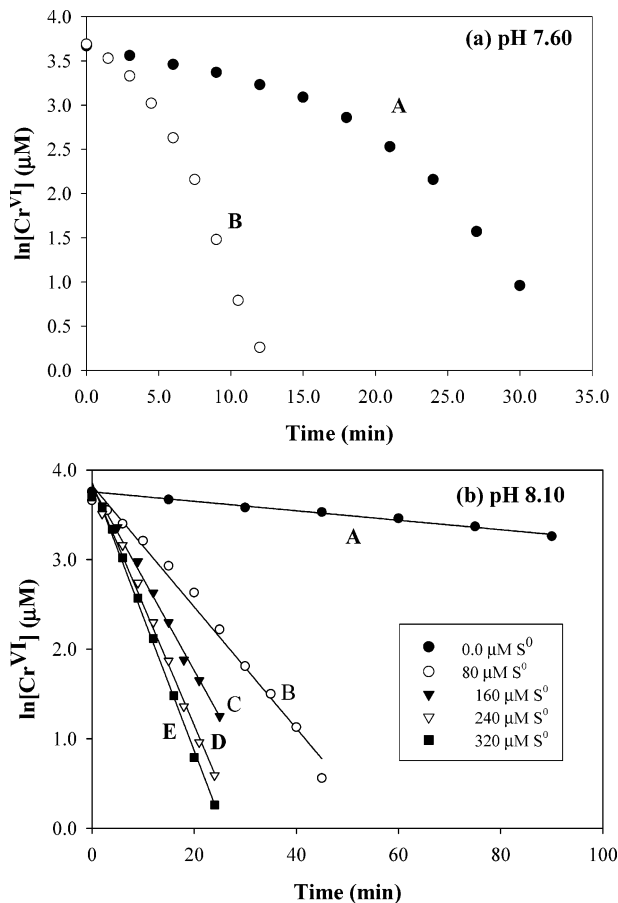


FIGURE 6. Effect of externally added elemental sulfur on Cr^{VI} reduction in the systems with excess of sulfide ($800 \mu M$) at $25^\circ C$ and pH 7.60 (a) and 8.10 (b). Different curves are for different S^0 concentrations: (A) control with no S^0 added; (B) $80 \mu M$; (C) $160 \mu M$; (D) $240 \mu M$; (E) $320 \mu M$.

was re-spiked into the system following complete reduction of originally added Cr^{VI} , the time for near 100% reduction of the re-spiked Cr^{VI} was accomplished within approximately 11 min (curve B), less than half of the time for the original Cr^{VI} reduction. When the solution from the first batch of Cr^{VI} reduction was centrifuged and filtered, followed by re-spiking of both Cr^{VI} and S^{II} , the time for the Cr^{VI} reduction was increased compared to the system without solid separation, but still slightly faster than the first batch (curve C). Similarly, at pH 8.10 (Figure 5b), it took 210 min for the complete reduction of the first batch of Cr^{VI} (curve A) and only 56 min for the second batch (curve B). These faster reaction rates were observed under slightly lower reductant concentrations than in the first batch since no sulfide was re-spiked. By comparing the data in Figure 5a,b, it was also clear that the reaction rates for both the first and second batches at pH 8.10 were significantly slower than the rates at pH 7.60, agreeing with the general trend that the higher the acidity is, the faster the Cr^{VI} reduction (9, 15).

Another set of experiments involved adding various amounts of elemental sulfur particles into the system before the redox reaction was initiated. The results showed that the presence of elemental sulfur significantly increased the reaction rate at both pH 7.60 and pH 8.10 (Figure 6a,b). The time for complete Cr^{VI} reduction at pH 7.60 was decreased from longer than 32 min to approximately 12 min when $80 \mu M$ of elemental sulfur was added into the system at the beginning. At pH 8.10, various concentrations of elemental sulfur were externally added, which greatly decreased the

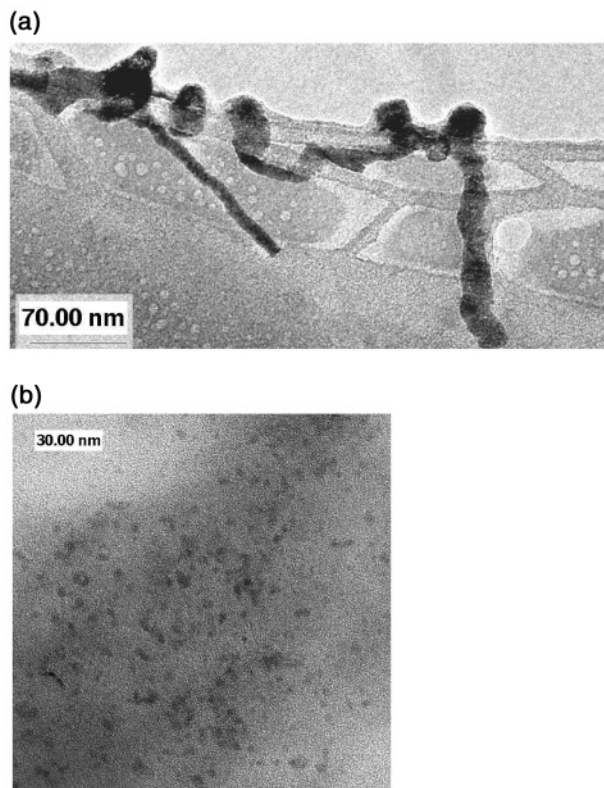


FIGURE 7. Bright-field TEM images of elemental sulfur. (a) S^0 particles from a sample without H_2S treatment. Most S particles display elongated shapes. Average width of the elongated S particles is about 10 nm. (b) S^0 nanoparticles from a sample with H_2S treatment. They are nanocrystalline particles. Noise background is amorphous carbon film holding the S particles. Average size of the S nanocrystals is about 5 nm.

time for complete Cr^{VI} reduction. The higher the concentrations of added sulfur particles, the faster the rates of Cr^{VI} reduction. When the initial concentration of elemental sulfur was raised to $320 \mu M$, the time needed for completing the reaction was less than 30 min. In addition, in the presence of externally added elemental sulfur particles, the $\ln [Cr^{VI}]$ vs t plots were nearly linear for the whole experimental time period, following a first-order kinetics with respect to Cr^{VI} (Figure 6b). This was different from the situation when elemental sulfur was only produced as a reaction product (Figure 2).

During the tests with externally added sulfur particles, we observed that the system exhibited a milky white appearance typical of elemental sulfur sols. When sulfide was also added into the system, this milky white appearance disappeared and the colloidal system became almost as clear as true solution. TEM study showed that, without S^{-II} in the system, the elemental sulfur particles displayed an elongated shape, with an averaged width of 10 nm and length of 50–100 nm (Figure 7a). With S^{-II} being present, the elemental sulfur was in the form of much smaller nanoparticles with an average size around 5 nm (Figure 7b). These S^0 nanoparticles were not amorphous, but in crystalline form because sharp diffraction rings in selected-area electron diffraction (SAED) patterns were observed. Apparently, interactions between S^0 nanoparticles and S^{-II} , or the sorption of S^{-II} onto the particle surfaces, had altered the crystalline and/or aggregation behavior of the elemental sulfur.

Effect of Dissolved Oxygen. As illustrated by Figure 8, when dissolved oxygen in the solution was not removed by

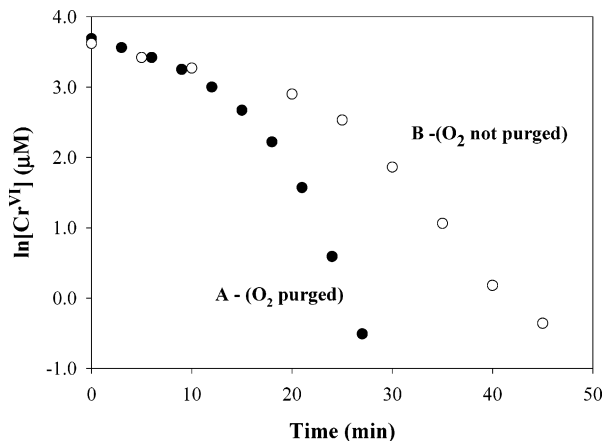


FIGURE 8. Effect of oxygen on the rate of Cr^{VI} reduction by sulfide ($[S^{-II}]_0 = 800 \mu M$; $pH = 7.60$; $25^\circ C$).

N_2 purging before the addition of Cr^{VI} and S^{-II} solutions, the time for complete Cr^{VI} reduction was increased in comparison to the system with purging. The amount of dissolved oxygen in the system without purging was determined to be approximately $63 \mu M$, and when purged, the dissolved oxygen was less than the detection limit of $6.3 \mu M$. Oxygen could affect the reaction by (i) oxidizing S^{-II} species and/or (ii) oxidizing elemental sulfur products. While both mechanisms might contribute to the effect, we believe that the second mechanism was likely the dominant one. The maximum amount of oxygen in the system was much less than S^{-II} , so even all oxygen was consumed for sulfide oxidation to elemental sulfur, S^{-II} concentration still remained almost the same, within 84% of its original value of $800 \mu M$. The rate difference with and without oxygen was much larger than the modest change of S^{-II} concentration. On the contrary, consumption of elemental sulfur due to oxygen could significantly decrease its catalytic effect and decrease the reaction rate, because the elemental sulfur product was in a much smaller amount. The concentration profiles also showed that, only at the later stage of the reaction when the effect of elemental sulfur was significant, the effect became more pronounced.

Effect of Temperature. Temperature effect was examined at 5, 10, 25, and $35^\circ C$ ($pH 7.60$), and data analysis was focused on the initial stage of the reaction (0–15 min) when the reaction followed the pseudo-first-order kinetics. The $\log k$ vs $1/T$ plot was linear for the reaction between Cr^{VI} and S^{-II} , from which an activation energy of 35.4 ± 14.5 kJ/mol was calculated. This value was comparable to the 43.6 ± 1.5 kJ/mol obtained from a similar experimental system (7).

Discussion

The stoichiometry of Cr^{VI} to S^{-II} is 1:1.5 under various concentration ratios (Table 1), indicating that elemental sulfur is the product of sulfide oxidation under the anaerobic condition and the reaction stoichiometry follows eq 1. This agrees with the result previously reported, where the elemental sulfur is directly detected by TEM with associated X-ray energy dispersion spectrometry (EDS) (9). Sulfate is not detected under the experimental conditions. Elemental sulfur is therefore the only major product for sulfide oxidation by Cr^{VI} under the anaerobic condition.

The rate for Cr^{VI} reduction is pseudo first order based on calculations using the initial rate method. Strictly speaking, this reaction order applies only when the reaction time is close to zero. Nevertheless, the data as presented in Figure 2 indicate that the first-order kinetics has extended until approximately 40% of Cr^{VI} is reduced. When the data collected within the first 15 min are used, $\ln [Cr^{VI}]$ vs t plots are all

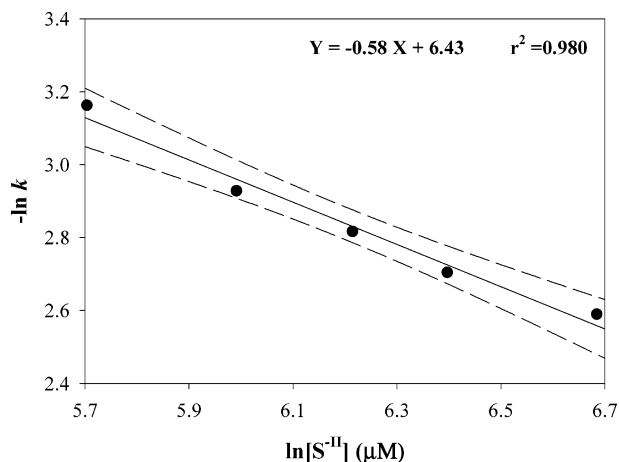


FIGURE 9. $-\ln k$ vs $\ln [\text{H}_2\text{S}]$ plot used for the calculation of reaction order with respect to $\text{S}^{-\text{II}}$ ($[\text{Cr}^{\text{VI}}]_0 = 20 \mu\text{M}$; $\text{pH} = 7.60$; 25°C). Dashed lines represent the 95% confidence level.

linear with $R^2 > 0.98$. Slopes of these $\ln [\text{Cr}^{\text{VI}}]$ vs t plots, i.e., the pseudo-first-order rate constants under various initial Cr^{VI} concentrations (from 20 to $60 \mu\text{M}$), are 0.034, 0.040, 0.040, 0.041, and 0.039 min^{-1} , respectively, with an average of $0.039 \pm 0.004 \text{ min}^{-1}$. Using a pseudo-first-order kinetics for Cr^{VI} , the overall rate equation can be written as

$$-\frac{d[\text{Cr}^{\text{VI}}]}{dt} = k_1[\text{Cr}^{\text{VI}}][\text{H}_2\text{S}]^a_T \quad (2)$$

Under excess $\text{S}^{-\text{II}}$ over Cr^{VI} , eq 3 can be rewritten as

$$-\frac{d[\text{Cr}^{\text{VI}}]}{dt} = k_2[\text{Cr}^{\text{VI}}] \quad (3)$$

where $k_2 = k_1[\text{H}_2\text{S}]^a_T$. With $k_2 = 0.039 \text{ min}^{-1}$ and $a = 0.67$ as previously calculated by the initial rate method, we get $k_1 = 4.4 \times 10^{-4} (\mu\text{M})^{-0.67} \text{ min}^{-1}$ in the system with $[\text{S}^{-\text{II}}]_0 = 800 \mu\text{M}$ ($\text{pH} 7.60$; 25°C).

The reaction order with respect to $[\text{S}^{-\text{II}}]_0$, a , can also be determined by plotting $\ln k_2$ versus $\ln [\text{S}^{-\text{II}}]_0$, when k_2 is obtained by $\ln [\text{Cr}^{\text{VI}}]$ vs t plots using the data for Cr^{VI} reduction at the initial 15 min of reaction (figures not shown). Since the concentration of sulfide is at least 15 times higher than the Cr^{VI} concentration, i.e., $[\text{S}^{-\text{II}}]_0 \approx [\text{S}^{-\text{II}}]_T$ during the reaction, this approach can be justified. As shown in Figure 9, the reaction order determined following this procedure is 0.58 ± 0.15 (95% confidence level), very close to the 0.67 calculated by the initial rate method, with a rate constant $k_1 = 1.6 \times 10^{-3} (\mu\text{mol/L})^{-0.58} \text{ min}^{-1}$. Since the reaction order (a) and the rate constant (k_1) calculated using both the initial rate method and the integrated kinetic equation are essentially the same statistically, we will use the average of 0.63 for a and $1.0 \times 10^{-3} (\mu\text{M})^{-0.63} \text{ min}^{-1}$ for k_1 for the kinetic presentation of the system.

The reaction order with respect to $[\text{S}^{-\text{II}}]_0$ is lower than unity reported in the literature (7, 9). A plausible reason is that the anaerobic condition in this study is more strictly controlled by conducting all tests in the anaerobic chamber, which is more effective than by N_2 -gas purging of the reaction systems used in the previous studies. The exact mechanism leading to the fractional order with respect to $\text{S}^{-\text{II}}$ is unclear. Such fractional order has been, however, frequently observed in sulfide oxidation by oxygen (25), but the underlying mechanisms are likely different because no oxygen is present in our systems.

For the rate acceleration at the later stage of the reaction, we believe that it is caused by S^0 nanoparticles produced in the system. Several lines of evidence support this hypothesis.

First, re-spiked Cr^{VI} is reduced much faster than the reduction of Cr^{VI} originally present in the system. Because one of the two main reaction products, $\text{Cr}(\text{OH})_3(\text{s})$, does not affect the reaction, the other one, S^0 , is most likely involved. Second, the presence of externally added S^0 increases the rate of Cr^{VI} reduction, and the higher the S^0 concentration, the faster the rate (Figure 6b). Interpretation of the experiment with centrifugation and filtration for S^0 removal is less definite. Although S^0 in the system without $\text{S}^{-\text{II}}$ can be easily separated by centrifugation and filtration, in the presence of $\text{S}^{-\text{II}}$, externally added S^0 particles are dispersed as nanoparticles with diameters around 5 nm, and thus separation through filtration is unlikely to be complete. On the other hand, the centrifugation/filtration process takes up to 40 min and is performed in ambient air. Sulfur oxidation by oxygen and its adsorption onto the membrane can certainly occur to a certain degree, which may enhance S^0 removal. Nevertheless, the reduction rate of re-spiked Cr^{VI} (curve C in Figure 5a) is significantly slower than that without elemental sulfur removal but slightly faster than the first batch of Cr^{VI} , suggesting that elemental sulfur nanoparticles are partially destroyed.

The catalysis caused by S^0 produced during the reaction cannot be modeled by a typical autocatalytic model (40, 41). The rate of a typical autocatalytic reaction is slow initially, increases to a maximum, and decreases again due to the depletion of the reactants. For example, oxidation of organic compounds by MnO_4^- follows this autocatalytic model, in which Mn^{2+} produced during the reaction acts as a catalyst (40, 41). The kinetic data on Cr^{VI} reduction by sulfide in our system, however, does not follow this typical autocatalytic model. Instead, the reaction follows first-order kinetics at the initial stage of the reaction, up to 40% of Cr^{VI} reduction (Figure 2). The acceleration takes place only after approximately 15 min of reaction, and by that time, the amount of S^0 produced can be as high as $40 \mu\text{M}$. This is not consistent with the polysulfides being responsible for the enhanced reaction, although polysulfides have been considered to be more reactive than HS^- for certain reactions (42, 43).

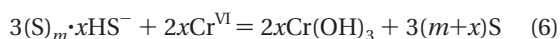
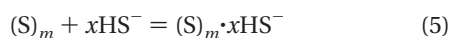
We propose that elemental sulfur nanoparticles are the catalyst of Cr^{VI} reduction by sulfide. Elemental sulfur, when first produced during the reaction, is dispersed as individual molecules in the aqueous system and/or in polysulfide (primarily S_4^{2-} and S_5^{2-}) forms and is not capable of catalyzing the reaction. Only when nucleation occurs that eventually leads to the formation of crystalline S^0 nanoparticles, the catalytic pathway becomes significant compared to the noncatalytic pathway. Thus, the reaction follows the pseudo-first-order kinetics at the initial stage when the elemental sulfur nanoparticles are not significant, even though an individual S^0 molecule is produced from the very beginning of the reaction and some polysulfides may also be present. Once S^0 nanoparticles, which provide reactive surface for reactant adsorption, are formed, the reaction is accelerated due to the high reactivity of sorbed sulfide on the particles. Higher initial Cr^{VI} concentration results in a larger acceleration at the later stage, which is likely due to a larger amount of elemental sulfur product that encourages S^0 nanoparticles formation. Adsorption of Cr^{VI} onto amorphous elemental sulfur is insignificant (less than 3%). $\text{S}^{-\text{II}}$ sorption onto S^0 nanoparticles, however, is highly likely due to the similar electronic structures of S^0 and $\text{S}^{-\text{II}}$. The particle size of elemental sulfur is significantly decreased due to the presence of $\text{S}^{-\text{II}}$, as shown in Figure 7, which indicates the existence of strong interactions between S^0 and $\text{S}^{-\text{II}}$. Our effort of measuring $\text{S}^{-\text{II}}$ sorption onto the elemental sulfur colloids, however, was not successful because we were unable to completely separate solids with particle sizes around 5 nm.

TABLE 3. Rate Constants, k_1 and k_2 , for the Direct Aqueous-Phase Reaction and k_3 and k_4 for the Catalyzed Pathway, Calculated According to the Experiments with Externally Added Colloidal Sulfur at pH 8.10 and 25 °C^a

colloidal sulfur (μM)	k_1 (μM) ^{-0.63} min ⁻¹	k_2 (min ⁻¹)	k_3 (μM) ^{-0.57} min ⁻¹	$k_2 + k_4$ (min ⁻¹)	k_4 (min ⁻¹)	b
80	8.2×10^{-5}	0.0053	0.0057	0.0679	0.0626	0.57
160				0.1028	0.0975	
240				0.1347	0.1294	
320				0.1498	0.1445	

^a Parameter b represents the reaction order for adsorbed sulfide ($[\text{S}^{\text{II}}]_0 = 800 \mu\text{M}$; $[\text{Cr}^{\text{VI}}]_0 = 40 \mu\text{M}$).

With such understanding, we propose the following reaction scheme for the catalytic Cr^{VI} reduction by the elemental sulfur produced during the reaction:



where the first step represents the formation of S⁰ nanoparticles, the second the sorption of S^{-II} onto the reactive surfaces, and the third the reduction of Cr^{VI} by the sorbed S^{-II}. Assuming that the rate of Cr^{VI} reduction through the catalytic pathway is proportional to the Cr^{VI} concentration and the adsorbed amount of S^{-II}, the overall rate equation including both noncatalytic and catalytic pathways can be expressed as

$$\begin{aligned} -\frac{d[\text{Cr}^{\text{VI}}]}{dt} &= k_1[\text{Cr}^{\text{VI}}][\text{H}_2\text{S}]_T^a + k_3[\text{Cr}^{\text{VI}}][\equiv\text{S}-\text{SH}]^b \quad (7) \\ &= (k_1[\text{H}_2\text{S}]_T^a + k_3[\equiv\text{S}-\text{SH}]^b)[\text{Cr}^{\text{VI}}] \\ &= (k_2 + k_4)[\text{Cr}^{\text{VI}}] \end{aligned}$$

where $[\equiv\text{S}-\text{SH}]$ represents the effective concentration of sulfide on the colloidal surfaces and b is the reaction order with respect to this effective concentration. The first term is corresponding to the noncatalytic pathway, with $k_1 = 1.0 \times 10^{-3} (\mu\text{mol/L})^{-0.63} \text{min}^{-1}$ and $a = 0.63$ at pH = 7.60 and 25 °C, as discussed earlier. The catalytic term, $k_3[\text{Cr}^{\text{VI}}][\equiv\text{S}-\text{SH}]^b$ is more important at the later stage of the reaction, based on the observed kinetics and the enhancement of the reaction rate by the addition of colloidal elemental sulfur.

The results in the systems with externally added S⁰ particles can be easily explained by eq 7; i.e., the reaction is pseudo first order with respect to Cr^{VI} (Figure 6b). k_2 , the rate constant corresponding to direct aqueous phase reaction, can be calculated from the $\ln[\text{Cr}^{\text{VI}}]$ vs t plot for the system without S⁰ addition. The sum of $k_2 + k_4$ can be obtained from the experiments with externally added S⁰. As indicated in Table 3, the rate constant for the surface reaction, k_4 , is 12–27 times larger than k_2 . Another conclusion can be obtained when k_1 and k_3 are compared. k_3 and b are determined on the basis of the relationship $k_4 = k_3[\equiv\text{S}-\text{SH}]^b$ (listed in Table 3). k_1 is calculated at pH 8.10 according to the relationship $k_2 = k_1[\text{H}_2\text{S}]^a$ with $a = 0.63$. The surface related constant, k_3 , is approximately 70 times larger than aqueous-phase rate constant k_1 . These results suggest that the elemental sulfur nanoparticles can dramatically enhance the rate of Cr^{VI} reduction. The effect of pH on the reaction can also be illustrated by the rate constants. For example, k_1 is increased

from 8.2×10^{-5} to $1.0 \times 10^{-3} (\mu\text{M})^{-0.63} \text{min}^{-1}$, or 12 times, when the pH is decreased from 8.10 to 7.60.

In summary, the reduction of Cr^{VI} by sulfide under anaerobic conditions is pseudo first order with respect to Cr^{VI} at the initial stage of the reaction. The reaction stoichiometry between Cr^{VI} and S^{-II} is 1:1.5, indicating the formation of elemental sulfur as the product of sulfide oxidation. When individual elemental sulfur molecules interact to form nanocrystalline sulfur particles, a new reaction pathway is created via the sorption of sulfide onto the elemental sulfur nanoparticles, and the rate of Cr^{VI} reduction is greatly increased. Nevertheless, this proposed mechanism should still be considered speculative, further study on the growth of elemental sulfur nanoparticles should be conducted to relate the speciation and the reactivity. In the presence of oxygen, the reaction occurs significantly slower compared to the anaerobic system, because the elemental sulfur is likely oxidized.

Acknowledgments

This research was supported by the Office of Science (BER), U.S. Department of Energy under the Environmental Management Science Program (Grant Nos. DE-FG07-99ER15011 and DE-FG02-03ER63616). TEM analyses were carried out at the Transmission Electron Microscopy Laboratory in the Department of Earth and Planetary Science of the University of New Mexico, which is supported by NSF, NASA, and the State of New Mexico.

Literature Cited

- Riley, R. G.; Zachara, J. M. *Chemical Contaminants on DOE Lands and Selection of Contaminant Mixtures for Subsurface Science Research*; U.S. Department of Energy: 1992.
- National Research Council. *Alternatives for Ground Water Cleanup*; National Academy Press: Washington, D.C., 1994.
- Seaman, J. C.; Bertsch, P. M.; Schwallie, L. In Situ Cr(VI) Reduction within Coarse-Textured, Oxide-Coated Soil and Aquifer Systems Using Fe(II) Solutions. *Environ. Sci. Technol.* **1999**, *33*, 938–944.
- Buerge, I. J.; Hug, S. J. Kinetics and pH Dependence of Chromium(VI) Reduction by Iron(II). *Environ. Sci. Technol.* **1997**, *31*, 1426–1432.
- Eary, L. E.; Rai, D. Chromate Removal from Aqueous Wastes by Reduction with Ferrous Ion. *Environ. Sci. Technol.* **1988**, *22*, 972–977.
- Fendorf, S. E.; Li, G. Kinetics of Chromate Reduction by Ferrous Iron. *Environ. Sci. Technol.* **1996**, *30*, 1614–1617.
- Pettine, M.; Millero, F. J.; Passino, R. Reduction of Chromium(VI) with Hydrogen Sulfide in NaCl Media. *Mar. Chem.* **1994**, *46*, 335–344.
- Thornton, E. C.; Amonette, J. E. Hydrogen Sulfide Gas Treatment of Cr(VI)-Contaminated Sediment Samples from a Plating-Waste Disposal Site. Implications for in-Situ Remediation. *Environ. Sci. Technol.* **1999**, *33*, 4096–4101.
- Kim, C.; Zhou, Q. H.; Deng, B. L.; Thornton, E. C.; Xu, H. F. Chromium(VI) Reduction by Hydrogen Sulfide in Aqueous Media: Stoichiometry and Kinetics. *Environ. Sci. Technol.* **2001**, *35*, 2219–2225.
- Wittbrodt, P. R.; Palmer, C. D. Reduction of Cr(VI) in the Presence of Excess of Soil Fulvic Acid. *Environ. Sci. Technol.* **1995**, *29*, 255–263.
- Elovitz, M. S.; Fish, W. Redox Interactions of Cr(VI) and Substituted Phenols: Kinetic Investigation. *Environ. Sci. Technol.* **1994**, *28*, 2161–2169.
- Deng, B.; Stone, A. T. Surface-Catalyzed Chromium(VI) Reduction: The TiO₂-Mandelic Acid System. *Environ. Sci., & Technol.* **1996**, *30*, 2486–2494.
- Deng, B.; Stone, A. T. Surface-Catalyzed Chromium(VI) Reduction: The TiO₂-Mandelic Acid System. *Environ. Sci. Technol.* **1996**, *30*, 463–472.
- Pettine, M.; D'Ottone, L.; Campanella, L.; Millero, F. J.; Passino, R. The Reduction of Chromium(VI) by Iron(II) in Aqueous Solutions. *Geochim. Cosmochim. Acta* **1998**, *62*, 1509–1519.
- Deng, B. Chromium(VI) Reduction by Naturally-Occurring Organic Compounds: Direct and Surface-Catalyzed Reactions.

- Ph.D. Dissertation, The Johns Hopkins University, Baltimore, MD, 1995; p 188.
- (16) Eary, L. E.; Rai, D. Kinetics of Chromium(III) Oxidation to Chromium(VI) by Reaction with Manganese Dioxide. *Environ. Sci. Technol.* **1987**, *21*, 1187–1193.
 - (17) Fendorf, S. E.; Zasoski, R. J. Chromium(III) Oxidation by δ -Manganese Oxide (MnO_2). 1. Characterization. *Environ. Sci. Technol.* **1992**, *26*, 79–85.
 - (18) Fendorf, S. E. Surface Reactions of Chromium in Soils and Waters. *Geoderma* **1995**, *67*, 55–71.
 - (19) Banerjee, D.; Nesbitt, H. W. Oxidation of Aqueous Cr(III) at Birnessite Surfaces: Constraints on Reaction Mechanism. *Geochim. Cosmochim. Acta* **1999**, *63*, 1671–1687.
 - (20) Buerge, I. J.; Hug, S. J. Influence of Mineral Surfaces on Chromium(VI) Reduction by Iron(II). *Environ. Sci. Technol.* **1999**, *33*, 4285–4291.
 - (21) Huber, C.; Haight, G. Oxidation of Manganese(II) by Chromium(VI) in the Presence of Oxalate Ion. *J. Am. Chem. Soc.* **1976**, *98*, 4128–4131.
 - (22) Ghosh, S. K.; Gould, E. S. Electron Transfer. 103. Reactions of Aqueous Chromium(IV). *Inorg. Chem.* **1989**, *28*, 1538–1542.
 - (23) Yao, W.; Millero, F. H. The Rate of Sulfide Oxidation by Delta Manganese Dioxide in Seawater. *Geochim. Cosmochim. Acta* **1993**, *57*, 3359–3365.
 - (24) Yao, W.; Millero, F. H. Oxidation of Hydrogen Sulfide by Mn(IV) and Fe(III) (Hydr)oxides in Seawater. *Geochemical Transformations of Sedimentary Sulfur*; ACS Symposium Series, Vol. 612; American Chemical Society: Washington, D.C., 1995; pp 260–279.
 - (25) Chen, K. Y.; Morris, J. C. Kinetics of Oxidation of Aqueous Sulfide by O_2 . *Environ. Sci. Technol.* **1972**, *6*, 529–537.
 - (26) Kleinjan, W. E.; De Keizer, A.; Janssen, A. J. H. Biologically Produced Sulfur. *Top. Curr. Chem.* **2003**, *230*, 167–188.
 - (27) Cline, J. D.; Richards, F. A. Oxygenation of Hydrogen Sulfide in Seawater at Constant Salinity, Temperature, and pH. *Environ. Sci. Technol.* **1969**, *3*, 838–843.
 - (28) Chadwell, S. J.; Rickard, D.; Luther, G. W., III. Electrochemical Evidence for Pentasulfide Complexes with Mn^{2+} , Fe^{2+} , Co^{2+} , Ni^{2+} , Cu^{2+} and Zn^{2+} . *Aquat. Geochem.* **1999**, *5*, 29–57.
 - (29) Chadwell, S. J.; Rickard, D.; Luther, G. W., III. Electrochemical Evidence for Metal Polysulfide Complexes: Tetrasulfide (S_4^{2-}) Reactions with Mn^{2+} , Fe^{2+} , Co^{2+} , Ni^{2+} , Cu^{2+} , and Zn^{2+} . *Electroanalysis* **2001**, *13*, 21–29.
 - (30) Steudel, R.; Eckert, B. Solid Sulfur Allotropes. *Top. Curr. Chem.* **2003**, *230*, 1–79.
 - (31) La Mer, V. K.; Dinegar, R. H. Theory, Production, and Mechanism of Formation of Monodispersed Hydrosols. *J. Am. Chem. Soc.* **1950**, *72*, 4847–4854.
 - (32) Steudel, R. Aqueous Sulfur Sols. *Top. Curr. Chem.* **2003**, *230*, 153–166.
 - (33) Pettine, M.; Barra, I.; Campanella, L.; Millero, F. J. Effect of Metals on the Reduction of Chromium(VI) with Hydrogen Sulfide. *Water Res.* **1998**, *32*, 2807–2813.
 - (34) APHA; AWWA; WPCF. *Standard Methods for the Examination of Water and Wastewater*; 20th ed.; American Public Health Association: Washington, D.C., 1998.
 - (35) Allen, H.; Fu, G.; Deng, D. Analysis of Acid-Volatile Sulfide (AVS) and Simultaneously Extracted Metals (SEM) for the Estimation of Potential Toxicity in Aquatic Sediments. *Environ. Toxicol. Chem.* **1993**, *12*, 1441–1453.
 - (36) Xu, H.; Wang, Y. Crystallization Sequence and Microstructure Evolution of Synroc Samples Crystallized from $\text{CaZrTi}_2\text{O}_7$ Melts. *J. Nucl. Mater.* **2000**, *279*, 100–106.
 - (37) Wilkins, R. G. *Kinetics and Mechanism of Reactions of Transition Metal Complexes*, 2nd ed.; VCH: New York, 1991.
 - (38) Swinbourne, E. S. *Analysis of Kinetic Data*; Appleton-Century-Crofts: New York, 1971.
 - (39) Schecher, W. D.; McAvoy, D. C. *MINEQL+, A Chemical Equilibrium Modeling System*, 4.0 ed.; Environmental Research Software: Hallowell, ME, 1998.
 - (40) Cappellos, C.; Bielski, B. *Kinetics Systems—Mathematical Description of Chemical Kinetics in Solution*; Krieger: New York, 1980.
 - (41) Schwartz, L. M. More on Autocatalytic Reaction Data Analysis. *J. Chem. Educ.* **1989**, *66*, 677–678.
 - (42) Steudel, R. Inorganic Polysulfides S_n^{2-} and Radical Anions $\text{S}_n^{\cdot -}$. *Top. Curr. Chem.* **2003**, *231*, 127–152.
 - (43) Roberts, A. L.; Sanborn, P. N.; Gschwend, P. M. Nucleophilic Substitution Reactions of Dihalomethanes with Hydrogen Sulfide Species. *Environ. Sci. Technol.* **1992**, *26*, 2263–2274.

Received for review July 27, 2004. Revised manuscript received December 19, 2004. Accepted December 22, 2004.

ES048829R